

Spitzer observations of the Orion OB1 association: disk census in the low mass stars

Jesús Hernández^{1,2}, Nuria Calvet¹, C. Briceño², L. Hartmann¹, A. K. Vivas², J. Muzerolle³, J. Downes^{2,4}, L. Allen⁵, R. Gutermuth⁵

hernandj@umich.edu

ABSTRACT

We present new *Spitzer Space Telescope* observations of two fields in the Orion OB1 association. We report here IRAC/MIPS observations for 115 confirmed members and 41 photometric candidates of the ~ 10 Myr 25 Orionis aggregate in the OB1a subassociation, and 106 confirmed members and 65 photometric candidates of the 5 Myr region located in the OB1b subassociation. The 25 Orionis aggregate shows a disk frequency of 6 % while the field in the OB1b subassociation shows a disk frequency of 13 %. Combining IRAC, MIPS and 2MASS photometry we place stars bearing disks in several classes: stars with optically thick disks (class II systems), stars with an inner transitional disks (transitional disk candidates) and stars with “evolved disks”; the last exhibit smaller IRAC/MIPS excesses than class II systems. In all, we identify 1 transitional disk candidate in the 25 Orionis aggregate and 3 in the OB1b field; this represents $\sim 10\%$ of the disk bearing stars, indicating that the transitional disk phase can be relatively fast. We find that the frequency of disks is a function of the stellar mass, suggesting a maximum around stars with spectral type M0. Comparing the infrared excess in the IRAC bands among several stellar groups we find that inner disk emission decays with stellar age, showing a correlation with the respective disk frequencies. The disk emission at the IRAC and MIPS bands in several stellar groups indicates that disk dissipation takes place faster in the inner region of the disks. Comparison with models of irradiated accretion

¹Department of Astronomy, University of Michigan, 830 Dennison Building, 500 Church Street, Ann Arbor, MI 48109, US

²Centro de Investigaciones de Astronomía, Apdo. Postal 264, Mérida 5101-A, Venezuela

³Steward Observatory, University of Arizona, 933 North Cherry Avenue, Tucson, AZ 85721, US

⁴Escuela de Física, Universidad Central de Venezuela, Apdo. Postal 47586, Caracas 1041-A, Venezuela

⁵Harvard-Smithsonian Center for Astrophysics, 60 Cambridge, MA 02138, US

disks, computed with several degrees of settling, suggests that the decrease in the overall accretion rate observed in young stellar groups is not sufficient to explain the weak disk emission observed in the IRAC bands for disk bearing stars with ages 5 Myr or older; larger degrees of dust settling are necessary to explain these objects.

Subject headings: infrared: stars: formation — stars: pre-main sequence — open clusters and associations: individual (Orion OB1 association) — protoplanetary systems: protoplanetary disk

1. Introduction

Observational and theoretical studies indicate that important processes in the evolution of protoplanetary disks take place at ages between 1 and 10 Myr. About 90% of the low mass stars (\sim K5 or later) have lost their primordial disks at 5-7 Myr (e.g., Haisch et al. 2001; Hartmann 2005; Hernández et al. 2007). Grains grow to sizes of \sim 1000 km stirring up the leftover small objects in the disks and originating the first generation of reprocessed dust by collisional cascades (Kenyon et al. 2005; Hernández et al. 2006). Giant planets are expected to form in this period (Pollack et al. 1996; Alibert et al. 2004). However, additional studies of disk population in this crucial age range are necessary to improve our knowledge and clarify many details about the evolution from primordial disks to planetary systems.

OB associations are excellent laboratories for comparative studies of protoplanetary disk evolution, because they harbor young stellar populations (1-10 Myr) originating from the same giant molecular clouds, spanning a wide range of stellar masses, and in a variety of evolutionary stages and environments (Brown et al. 1999; Sicilia-Aguilar et al. 2006; Briceño et al. 2007a; Preibisch & Zinnecker 2006). In particular, the Orion OB1 association (Ori OB1), as other OB associations, shows a well defined age sequence suggesting a large-scale triggered star formation scenario (Briceño et al. 2005, 2007a; Lee & Chen 2007). Ori OB1 contains very young subgroups (ages \lesssim 1 Myr) still embedded in their natal gas (e.g., Orion A and B clouds; Megeath et al. 2006), subgroups in the process of dispersing their natal gas (e.g., the σ Orionis cluster, age \sim 3 Myr; Hernández et al. 2007) and more evolved populations, which have long since dissipated their progenitor molecular clouds (e.g., the 25 Orionis aggregate, age \sim 10 Myr; Briceño et al. 2007b).

We are carrying out an optical photometric and spectroscopic survey of ~ 128 deg^2 in Ori OB1 in order to identify the low and intermediate mass stellar populations, and study the properties linked to the first stages of star and disk evolution (Briceño et al. 2001, 2005,

2007b,c; Calvet et al. 2005a; Hernández et al. 2005, 2006, 2007). In this work, we expand the results from the optical survey with the capabilities of the *Spitzer Space Telescope* at near and mid infrared wavelengths to identify and characterize protoplanetary disks around young stellar objects (e.g. Allen et al. 2004; Megeath et al. 2004; Gutermuth et al. 2004; Muzerolle et al. 2004; Hartmann et al. 2005; Sicilia-Aguilar et al. 2006; Hernández et al. 2007). In particular we study the near and mid infrared properties of stars in two IRAC/MIPS *Spitzer* fields encompassing an area of ~ 2.5 deg². One field is located in the 7-10 Myr 25 Orionis stellar aggregate (Briceño et al. 2007b), the most populous ~ 10 Myr stellar group known within 500 pc; the other is located in the Ori OB1b sub-association, in which we have estimated an age of ~ 5 Myr (Briceño et al. 2005, 2007b; Hernández et al. 2006). Additional results from the 3 Myr σ Orionis cluster (Hernández et al. 2007), also located in the Ori OB1b subassociation, allow us to cover most of the potentially crucial age range in protoplanetary disk evolution. In this cluster, we found 336 photometric members using optical and near infrared color-magnitude diagrams, about a third of this sample exhibits excess in the IRAC and/or MIPS bands indicating that they have disks.

This paper is organized as follows. In §2 we present the observational data and a brief description about membership. We analyze the observations and describe the disk emission detection in §3. The main results are summarized in §4.

2. Observations

2.1. Infrared photometry

We have obtained near-infrared (NIR) and mid-infrared photometry of two regions in the Orion OB1 association using the four channels (3.6, 4.5, 5.8 & 8.0 μm) of the InfraRed Array Camera (IRAC, Fazio et al. 2004), and the 24 μm band of the Multiband Imaging Spectrometer (MIPS; Rieke et al. 2004), on board the *Spitzer Space Telescope*. The field located in the 25 Orionis aggregate (hereafter “25 Orionis”) covers an area of ~ 1.1 deg² centered at RA ~ 5.42 hours and DEC ~ 1.64 deg; the other field (hereafter “OB1b”) covers an area of ~ 1.4 deg² on the Orion OB1b sub-association centered at RA ~ 5.52 hours and DEC ~ 1.71 deg. Dust infrared emission maps (Schlegel et al. 1998) reveal that at least 90% of the regions covered by IRAC images in 25 Orionis and OB1b have visual extinctions smaller than $A_V \sim 0.12$ and $A_V \sim 0.6$, respectively (see Hernández et al. 2006). These values are mostly in agreement with the mean visual extinction calculated from individual stars in Briceño et al. (2005).

The IRAC observations were done using a standard raster map with 290” offsets, to pro-

vide maximum areal coverage with just a slight overlap between frames, to aid in mosaicking the data. Each position is composed of 3 dithers, with a single-frame integration of 12 seconds. The IRAC observations were processed using the *IRACproc* (Schuster et al. 2006) package to create the final mosaics with a scale of 0.86 "/pixel (see Hernández et al. 2006). Point source detections were carried out individually on each IRAC channel using PhotVis tool (an IDL GUI-based photometry visualization tool developed by R. Gutermuth). More than 20,000 sources in each field were detected in at least one *Spitzer* band. We extracted the photometry of these objects using the *apphot* package in IRAF, with an aperture radius of 3".7 and a background annulus from 3.7 to 8".6. We adopted zero-point magnitudes for the standard aperture radius (12") and background annulus (12-22".4) of 19.665, 18.928, 16.847 and 17.391 in the [3.6], [4.5], [5.8] and [8.0] channels, respectively. Aperture corrections were made using the values described in IRAC Data Handbook (Reach et al. 2006).

MIPS observations were obtained using the medium scan mode with full-array cross-scan overlap, resulting in a total effective exposure time per pointing of 40 seconds. The images were processed using the MIPS instrument team Data Analysis Tool (DAT), which calibrates the data and applies a distortion correction to each individual exposure before combining it into a final mosaic (Gordon et al. 2005). We obtained point source photometry at 24 μm with IRAF/it daophot point spread function fitting, using an aperture size of about 5.7" and an aperture correction factor of 1.73 derived from the STinyTim PSF model. The absolute flux calibration uncertainty is less than 5%. Our final flux measurements are complete down to about 1 mJy in both maps (the limit flux is about 0.5 mJy).

Figures 1 and 2 show color images combining three channels of IRAC ([3.6],[4.5] and [8.0]) for 25 Orionis and for Ori OB1b, respectively. We display the low mass spectroscopic members from Briceño et al. (2005, 2007b,c) and the low mass photometric candidates selected in §2.3; the stars bearing disks studied in §3.1; and the intermediate mass members including the debris disk candidates and the Herbig Ae stars studied in Hernández et al. (2006).

2.2. Optical photometry

Optical (V and I Cousin) magnitudes were obtained from the CIDA Variability Survey which is being carried out using the QUEST I camera (Baltay et al. 2002) installed on the Jurgen Stock Telescope (a celar aperture 1-m Schmidt telescope) at the Venezuela National Astronomical Observatory. The camera, an array of 4x4 CCDs, is designed to work in driftscan mode, which is a very efficient way to survey large areas of the sky. Each scan was reduced and calibrated with the standard QUEST software and the method described

in Vivas et al. (2004), in which variable stars can be identified (see Briceño et al. 2005).

2.3. Low mass members and photometric candidates

We follow the procedures described in Hernández et al. (2007) to reject non stellar objects and contaminating sources using IRAC color-color and IRAC color-magnitude diagrams. In brief, we select stars with $[3.6] < 14.5$, below this limit, the contamination from extragalactic sources is expected to be more than 50% (Fazio et al. 2004). The $[4.5] - [5.8]$ versus $[5.8] - [8.0]$ and $[3.6] - [5.8]$ versus $[4.5] - [8.0]$ color-color diagrams were used to eliminate most of the galaxies with polycyclic aromatic hydrocarbon (PAH) emission and objects with strong $8 \mu\text{m}$ contamination (Gutermuth et al. 2007, in preparation).

Optical and 2MASS counterpart (Cutri et al. 2003) for the IRAC sources were found using a $2''$ matching radius. A preliminary list of 623 objects in 25 Orionis and 918 objects in OB1b were created using optical-2MASS color magnitude diagrams (V versus V-Ic, V versus V-J and J versus J-K) to select those objects above the zero age main sequence (ZAMS; Siess et al. 2000) at the distance of each stellar group (330 pc and 440 pc for 25 Orionis and OB1b, respectively; Briceño et al. 2005, 2007b; Hernández et al. 2005). We rejected by visual inspection non-members sources, like diffuse objects, and objects with an apparent problem in the photometry, like close binaries, faint companion binaries, and stars on the image border.

Low mass members were confirmed by Briceño et al. (2005, 2007b,c) using optical spectra obtained at the Fred Lawrence Whipple Observatory with the 1.5 m telescope equipped with the FAST spectrograph (Fabricant et al. 1998), and with the 6.5 m MMT telescope equipped with the Hectospec and Hectochelle multifiber spectrographs (Fabricant et al. 2005). Additional low resolution spectra were obtained at the Kitt Peak National Observatory using the Hydra multiobject spectrograph on the 3.5 m WIYN telescope. Low mass members of 25 Orionis and Ori OB1b can be identified by the presence of Li I $\lambda 6707$ in absorption and the equivalent width of the $H\alpha$ line in emission (e.g. Briceño et al. 1998). The strength of the $H\alpha$ line is used to separate accreting stars, the Classical T Tauri stars (CTTS), from non-accreting stars, the Weak T Tauri stars (WTTS). To distinguish between the two type of objects we followed the prescription adopted by White & Basri (2003). Spectral types were derived using the SPTCLASS code ¹, which includes several molecular features (like TiO and VO bands), characteristic of low mass stars. Some stars in our sample have additional spectroscopic confirmation using radial velocity distributions. We refer

¹<http://www.astro.lsa.umich.edu/~hernandj/SPTclass/sptclass/html>

the reader to Briceño et al. (2005, 2007b,c) for more details about spectroscopic membership confirmation of stars belonging to the Ori OB1 association. Tables 1 and 2 show the IRAC and MIPS photometry for 115 confirmed members of 25 Orionis and 106 confirmed members of Ori OB1b. Column 1 shows the internal running identification number in each sample, columns 2 shows the 2MASS designation (Cutri et al. 2003); columns 3 and 4 are the stellar coordinates; columns 5, 6, 7 and 8 give IRAC magnitudes in the bands [3.6], [4.5], [5.8] and [8.0], respectively; column 9 gives MIPS (24 μm) magnitudes; column 10 gives the reference for the optical spectroscopic and photometric data ; the last column gives the disk classification based on the IRAC and MIPS analysis (§3.1).

Figure 3 shows optical-2MASS color magnitude diagrams (CMDs), V vs V-I and V versus V-J, illustrating the selection of the photometric candidates of 25 Orionis (upper panel) and Ori OB1b (lower panels). Solid lines represent the ZAMS (Siess et al. 2000) for each stellar group. Dashed lines represent the 10 Myr and 5 Myr isochrones (Siess et al. 2000). Since, it is well-known that theoretical, non-birthline isochrones do not so well for intermediate mass stars (Hartmann 2003) and the opacity tables at low temperatures are incomplete (Lyra et al. 2006; Baraffe et al. 1998), these theoretical isochrones are plotted as reference and do not affect the selection of the photometric candidates. We assumed a distance of 330 pc for 25 Orionis and 440 pc for OB1b (Briceño et al. 2005, 2007b; Hernández et al. 2005). The distribution of confirmed members (open circles) can be roughly traced as a straight line in the CMD diagrams, with a larger spread in Ori OB1b due to the larger visual extinction in this region in comparison with 25 Orionis. We calculated the median colors (V-I and V-J) for confirmed members (open circles) within 1.0 mag bins in the visual band. We used the differences between the observed colors and the expected colors (the median; represented by long dashed lines) to calculate the standard deviation (σ) of the member samples. We selected as photometric candidates (open squares) stars located in the region described by the 2.5σ limits in the CMDs (see Hernández et al. 2007). Tables 3 and 4 show the IRAC, MIPS and optical photometry for the 41 photometric candidates found in 25 Orionis and for the 65 candidates found in OB1b, respectively. The information shown in these tables in columns from 1 to 9 is the same as in Table 1. Columns 10 and 11 show the V magnitude and the color V-I from the CIDA survey; the last column gives the disk classification based on the IRAC and MIPS analysis (§3.1).

3. Results

3.1. Disk diagnostics

Figures 4 and 5 show three diagrams used to identify and roughly characterize the stars bearing disks in 25 Orionis and OB1b, respectively. The top panels show the SED slope, determined from the [3.6]–[8.0] color (IRAC SED slope), versus the [8.0] magnitude for members (open circles) and photometric candidates (open squares). The photospheric level is described by the upper solid line, which is calculated using the photometric errors propagated from the [3.6]–[8.0] color (Hernández et al. 2007). Stars with excess emission at $8 \mu\text{m}$ can be identified in this diagram. For comparison, IRAC SED slope histograms for Taurus (Hartmann et al. 2005) and for the σ Orionis cluster (Hernández et al. 2007) are displayed. In general, disk bearing stars in Taurus (solid histogram) are located in a well defined region (which we call the class II region) with an IRAC SED slope > -1.8 (see Lada et al. 2006); this limit (dashed lines) is used to identify objects with optically thick disks in which the inner disk emission has not been affected significantly by evolutionary processes. In contrast, 15% of the disk bearing stars in the σ Orionis cluster exhibit smaller IRAC excesses (dashed histogram) suggesting a reduction in disk photosphere height, possibly due to dust growth and/or settling (Hernández et al. 2007). The bottom left panel shows the K–[24] versus V–J color-color diagram, in which we identify members (big open circles) and photometric candidates (big open squares) with $24 \mu\text{m}$ infrared emission above the photospheric level (solid lines) indicating that disks are present around these objects (e.g.; Gorlova et al. 2006; Hernández et al. 2006, 2007). In this panel, we display the K–[24] color distribution for stars bearing disks in the σ Orionis cluster with an IRAC SED slope > -1.8 (which represents a disk population similar to those found in Taurus) and we use this histogram to identify stars with K–[24] color characteristic of stars with optically thick disks ($\text{K}–[24] > 3.5$, class II region). In the upper panel and in the bottom left panel, we define the “evolved disk region” between the class II region and the photospheric region. The bottom right panel shows the IRAC color-color diagram, in which we identify stars with excess emission in the IRAC bands (e.g. Allen et al. 2004; Megeath et al. 2004; Hartmann et al. 2005; Sicilia-Aguilar et al. 2006; Hernández et al. 2007). The dashed box displays the colors predicted for CTTS of different accretion rates by the models of D’Alessio et al. (2005b). In general, the IRAC colors observed for disk bearing stars in Taurus are located in this region (Hartmann et al. 2005; Sicilia-Aguilar et al. 2006).

In the top panel of Figure 4, we identify six members and two photometric candidates located on the IRAC class II region; most of them are located near the class II limit possibly indicating that these objects have begun the process of clearing the inner primordial disk. Two members have very small IRAC excesses just above the photospheric region. These

objects, also located between the photospheric and the CTTS regions in the IRAC color-color diagram, have no MIPS detections and therefore it is not clear if the small excess observed at $8\ \mu\text{m}$ originates from PAH background contamination, by an unresolved companion, or by disks present around these stars (flagged as “disk[8]?” in Table 1). Of particular interest are the member 1a_1121 and the photometric candidate 1a_1626 which are located between the photospheric and the class II region in the V-J versus K-[24] diagram indicating that the outer disks around these objects are in a more evolved stage. Moreover these stars are also located on the photospheric region in the IRAC color-color diagram and in the IRAC SED slope diagram indicating that the inner disk has already dissipated and no disk emission can be detected at wavelength $\lesssim 8\ \mu\text{m}$. The star 1a_1626 also has a very small excess at $24\ \mu\text{m}$ ($\sim 2\ \sigma$ above the photospheric level) indicating that the presence of a disk around this object is not yet conclusive. Overall, in 25 Orionis we identify 7 stars with disks in the member sample (disk frequency $6.1\pm 2.3\%$), and 3 in the photometric candidate sample (disk frequency $7.3\pm 4.2\%$).

Similarly, in the top panel of Figure 5 we identify 13 members and 4 photometric candidates in Ori OB1b that show IRAC and MIPS excesses; five of these objects are located between the class II region and the photospheric region. Eight members and one photometric candidate with no MIPS detection are located in the evolved disk region (flagged as “disk[8]?” in Table 2 and 4). The existence of disks around these objects needs additional confirmation since they could be below the MIPS detection limit, or could be contaminated by PAH background emission (in Figure 2 it can be clearly seen that the sky background emission at $8\ \mu\text{m}$ is very patchy, and significant at some locations). In general, the range of infrared excesses at $24\ \mu\text{m}$ in OB1b is similar to that of the optically thick disks in the σ Orionis cluster. Only one disk bearing star (6%), the star 1b_337, has $24\ \mu\text{m}$ excess below the class II limit while 6 stars (39%) have $8\ \mu\text{m}$ excess below this limit. This suggests a more rapid decrease in dust emission in the inner disk, in agreement with results from Sicilia-Aguilar et al. (2006) in the Cepheus OB2 association. The member 1b_337, located in the evolved disk region in the V-J versus K-[24] diagram, does not have excess in the IRAC bands. Overall, in Ori OB1b we identify 14 stars with disks in the member sample (disk frequency $13.1\pm 3.5\%$) and the 4 disk systems in the photometric candidate sample (disk frequency $6.2\pm 3.1\%$).

Figure 6 displays the distribution of the disk bearing stars in a SED slope space diagram for 25 Orionis (left panel) and OB1b (right panel). The vertical axis is the SED slope calculated from the K-[5.8] color and the horizontal axis is the SED slope calculated from the K-[24] color. The dashed areas define the photospheric level calculated with the STAR-PET *Spitzer* tool for stars K5 or later. By comparison the low mass stars bearing disks of the 3 Myr σ Orionis cluster (Hernández et al. 2007) are also plotted. Error bars represent the

quartiles of disk bearing stars in Taurus, calculated from the $K-[5.8]$ color in Hartmann et al. (2005) and from the $K-[24]$ color estimated from the median SED slope in Furlan et al. (2006), in the σ Orionis cluster from Hernández et al. (2007), in 25 Orionis and in Ori OB1b from this work. An overall decrease in the infrared excess is observed from the 1 Myr old stars in Taurus to the 5 and 10 Myr old stars studied in this work; the disk population of the 3 Myr σ Orionis cluster represents an intermediate stage in this evolution. Moreover, it is apparent that the decrease is larger at $5.8 \mu\text{m}$ than at $24 \mu\text{m}$, indicating that evolution processes occur faster in the inner region of the disk.

In order to characterize the stars bearing disks in 25 Orionis and OB1b, we identify several regions in Figure 6 defined by the dotted lines (“class II region”, “evolved disk region” and “transitional disk region”). The horizontal dotted line represents the lower quartile of the σ Orionis cluster. Above this line $\sim 96\%$ of the stars bearing optically thick disks in Taurus are also located, indicating a limit where the inner disk emission has not been affected significantly by evolutionary process. We can identify the class II objects as stars located above this line. In general, the class II objects identified using Figure 6 are located in the class II region in Figures 4 and 5. Disk bearing stars below the dotted lines have decreased the disk infrared emission at $5.8 \mu\text{m}$ due to a decrease in the irradiation surface of the inner disks, and so they are in an stage where processes for inner disk dissipation have begun. The vertical dotted line represents the lower quartile of the stars bearing disks in the σ Orionis cluster (the lower quartile of Taurus is rightward from this line). Using this limit, the stars located below the dotted lines could be sub-grouped based on their disk emission at $24 \mu\text{m}$: “evolved disks objects” ($\text{SED slope } K-[24] \lesssim -1.2$), in which we see an overall decrease in the disk emission in the IRAC and MIPS bands, indicating similar evolution in the inner and outer disk (Lada et al. 2006; Hernández et al. 2007); and “transitional disk candidates” ($\text{SED slope } K-[24] \gtrsim -1.2$), which have an inner optically thin disk region, combined with an outer, optically thick disk (e.g.; Calvet et al. 2005b). As reference, we plotted 3 transitional disk stars, Coku Tau/4 (D’Alessio et al. 2005a), TW Hya (Calvet et al. 2002; Uchida et al. 2004), GM Aur (Calvet et al. 2005b), which occupy the region defined for the “transitional disk candidates”. In brief, we identify 5 stars with optically thick disks (class II objects), one transitional disk candidate and 4 evolved disk objects in 25 Orionis. We also identify 10 class II objects, 3 transitional disk candidates and 5 evolved disk objects in OB1b. In spite of the evolved disks and transitional disks objects being a subsequent stage from class II objects, it is not clear if transitional disk objects are a pre-stage of evolved disks or each stage represents an independent stage from class II objects.

Figure 7 shows SEDs for selected stars in our samples illustrating the disk classification based on Figure 6. The first row of SEDs shows stars with optically thick disks (CII) located above the dotted line in Figure 6. The second row shows transitional disk candidates (TD)

located right and below the dotted lines in Figure 6. Finally, last two rows of panels show stars with evolved disks located left and below the dotted lines in Figure 6.

3.2. Models

We have calculated SED slopes for models of irradiated accretion disks including dust settling from D’Alessio et al. (2006). In these models the disk is assumed to be steadily accreting at rates of $\dot{M} = 1\text{e-}9, 1\text{e-}8, \text{ and } 1\text{e-}7 \text{ M}_\odot/\text{yr}$, onto a star with mass of 0.6 M_\odot and luminosity of 1.2 L_\odot , which corresponds to a K7 star with age of 1 Myr (Siess et al. 2000). Dust settling was included using two populations of grains (big and small grains) having different spatial distributions, with the larger grains concentrated toward the midplane. The small grains located in the upper layers have different depletions given by the ϵ parameter (with values= 1, 0.1, 0.01, 0.001), which is the ratio of the dust to gas mass ratio of small grains relative to the the standard dust to gas mass ratio ($\zeta_{small}/\zeta_{std}$; D’Alessio et al. 2006). The inner wall of the disk, located at the dust destruction radius, was settled self-consistently with the same degree of depletion used in the outer disk.

Figure 8 shows the theoretical SED slopes derived from the colors, [3.6]–[8.0], K–[5.8] and K–[24] versus the degree of settling represented by ϵ . SED slopes were calculated convoluting the theoretical SED with the transmission curves of the respective filters. We plot two inclination angles along the line of sight, 30 deg (left panels) and 60 deg (middle panels); this range in angles represents 40% of probability of observation. Accretion rates are indicated for the different curves plotted in each panel. The slope has a strong dependency on \dot{M} , showing flatter slopes for the fastest accretors; the smallest variation in disk emission with \dot{M} is observed for the slope K–[24] of disks without settling ($\epsilon=1$). In general, models with $\dot{M} = 10^{-9} \text{ M}_\odot/\text{yr}$ show a stronger dependence with dust settling than models for large accretion rates.

By comparison, we plotted in the right panels of Figure 8 the quartiles observed for disk bearing stars in Taurus, in the σ Orionis cluster, in Ori OB1b and in 25 Orionis. The range of disk emission observed in Taurus (1-2 Myr) can be explained by the models, indicating optically thick disks systems with several degrees of settling (Furlan et al. 2006) and accretion rates (Hartmann et al. 1998; Calvet et al. 2005a). Most of the stars with disks in the σ Orionis cluster ($\sim 80\%$) can be explained by the theoretical SED slopes but with small accretion rates or/and higher degree of dust settling than in Taurus. Approximately half of the disks observed in 25 Orionis (Figure 4) and OB1b (Figure 5) require models with lower accretion rates ($\dot{M} < 10^{-9} \text{ M}_\odot/\text{yr}$) or/and large degree of settling ($\epsilon < 0.001$) to explain the weak disk emissions observed at [3.6]–[8.0] and K–[5.8]. However, $\sim 75\%$ of disk

bearing stars in 25 Orionis and OB1b have disk emissions at K–[24] in agreement with the SED slopes predicted by the models, supporting the scenario where the inner disk evolves faster than the outer disk.

3.3. Disk frequencies

In Figures 4, 5 and 6 we identify 7 members bearing disks in 25 Orionis and 14 in Ori OB1b, indicating disks frequencies in the member samples of $6.1 \pm 2.3\%$ and $13.1 \pm 3.5\%$, respectively. These frequencies include objects with 24 μm excess as disk bearing stars. In §3.1, we also identify 2 members of 25 Orionis and 8 members of Ori OB1b that exhibit IRAC excesses but have no MIPS detections; if we add these stars as members with disks, the disk frequencies increase to $7.8 \pm 2.6\%$ in 25 Orionis and to $20.6 \pm 4.4\%$ in Ori OB1b. These later values are in better agreement with the disk frequencies calculated for the low mass stars in the Ori OB1a ($7 \pm 3\%$) and Ori OB1b ($17 \pm 4\%$) sub associations, using the excess emission (2σ above the expected photospheric level) from the 2MASS color H-K (Hernández et al. 2005). The lower disk frequencies derived using the 24 μm excess could indicate a possible observational bias produced by the flux limit of MIPS observations (~ 0.5 mJy). Assuming the distances and ages (Siess et al. 2000) plotted in Figure 3, with a visual extinction of $A_V=0.12$ mag for 25 Orionis and $A_V=0.6$ mag for OB1b, we cannot expect to detect disks around a $0.6M_\odot$ star in the 25 Orionis group if $E_{[24]} \lesssim 2.5$, and if $E_{[24]} \lesssim 4.5$ for objects in Ori OB1b; where the excess ratio, $E_{[24]}$, is the ratio of the observed flux to the expected photospheric flux at 24 μm .

Using the stars identified as members with infrared excess in Figure 6, we plotted in Figure 9 the fraction of stars bearing disks versus spectral type for 25 Orionis (dotted line) and OB1b (dashed line). Error bars represent the statistical \sqrt{N} errors in our derived frequencies. Previous studies have indicated that the frequency of disks is strongly dependent on the stellar mass, showing larger frequencies in the TTS mass range (spectral types K and M) than in stars with higher masses (Lada & Lada 1995; Sicilia-Aguilar et al. 2005; Hartmann 2005; Hernández et al. 2005; Carpenter et al. 2006; Briceño et al. 2007a). Figure 9 also suggests that the disk frequency declines toward lower masses (spectral types later than M1) showing a maximum around K7-M1 stars in agreement with results for the 2-3 Myr cluster IC 348 by Lada et al. (2006). However, given the degree of uncertainty in each individual point in Figure 9, caused by the small number of disk bearing stars in each spectral type bin, plus the observational bias introduced by the limiting magnitude in the MIPS photometry, this result is not conclusive and additional data is necessary to confirm this trend.

Using Figure 6, the frequencies calculated for stars with evolved disks related to the total number of stars bearing disks in the σ Orionis cluster (15.6 ± 4.0 %), in Ori OB1b (27.8 ± 12.4 %) and in 25 Orionis (40 ± 20 %), indicate a clear trend toward more evolved disks in older stellar groups. The transitional disks candidates in these stellar groups are less frequent than evolved disks (8 ± 3 % for the σ Orionis cluster, 17 ± 10 % for OB1b and 10 ± 10 % for 25 Orionis), suggesting that the transitional disk phase is relatively fast or represents an independent and special stage in the disk clearing period of stars.

Disk frequencies of the sample members can be used to estimate the contamination level of non-members in the photometric candidates samples assuming that the photometric candidates bearing disks are actual members of young stellar groups. Since the overall disk frequencies of low mass members (6.1 ± 2.1 %) and low mass photometric candidates (7.3 ± 4.2 %) in 25 Orionis are similar, we can expect that photometric candidates sample have very low non-member contamination. Since the disk frequency calculated in OB1b for the photometric candidates (6.2 ± 3.1 %) is lower than the disk frequency of members (13.1 ± 3.5), we can expect that around 50% of the photometric candidates are not members of OB1b.

3.4. Disk evolution

The frequency of stars bearing disks in different stellar groups is a function of age, indicating a time scale for disk dissipation in low mass stars of 5-7 Myr (e.g., Haisch et al. 2001; Briceño et al. 2007a; Hernández et al. 2005, 2007). The results presented in §3.3 are in agreement with this trend. In addition to this decline in disk frequency, the amount of infrared disk emission also decreases with age. The top panel of Figure 10 shows the median SED slope derived from the color $[3.6] - [8.0]$ for disk bearing stars in stellar groups ranging in age from ~ 1 to ~ 10 Myr: 1-2 Myr (Taurus; Hartmann et al. 2005), 1-3 Myr (NGC 2264; Young et al. 2004), 2-3 Myr (IC348; Lada et al. 2006), 3 Myr (σ Orionis; Hernández et al. 2007), 4 Myr (Tr 37; Sicilia-Aguilar et al. 2006), 5 Myr (OB1b; Briceño et al. 2007b, and this work), 7-10 Myr (25 Orionis; Briceño et al. 2007b, and this work) and 10-12 Myr (NGC 7160; Sicilia-Aguilar et al. 2006). We estimated the photospheric level using the STAR-PET *Spitzer* tool for the star templates with spectral types between K5 to M5. Error bars represent the quartiles given the median value for each stellar group. The median SED slope decreases with age, indicating a reduction of disk emission the inner regions of the disk. In the bottom panel, we display two sets of models described in §3.2 with different disk orientations, $i=30$ deg (dashed lines) and $i=60$ deg (dotted lines). The accretion rate is a function of age (Hartmann et al. 1998; Muzerolle et al. 2000; Calvet et al. 2005a), so we

assumed $\dot{M}=10^{-8}M_{\odot}$ for 1 Myr old stellar groups, which is the mode value for accreting stars in Taurus (Hartmann et al. 1998) and $\dot{M}=10^{-9}M_{\odot}$ for 10 Myr old stellar groups, which is the mode value for accreting stars in the OB1a sub-association (Calvet et al. 2005a). This plot suggests that the expected decrease in accretion rate is not sufficient to explain the decrease of emission in the inner part of the disk, and it is necessary to increase the degree of settling ($\epsilon < 0.001$) in the inner disk to explain the observed slopes in stellar groups with ages 5 Myr or older.

Since the disk frequency and the infrared disk emission decrease with age, a correlation between these values can be expected. Figure 11 confirms this suggestion, showing that the disk frequency is correlated with the median SED slope in the IRAC bands (correlation coefficient $\rho=0.76$). This plot clearly demonstrates that the disappearance of inner disks is related to the decrease of optical depth in the inner disk due to the increase of dust settling and the decrease of mass accretion rate (see D’Alessio et al. 2006).

4. Conclusions

We have used the IRAC and MIPS data from *Spitzer* to study the disk frequencies and properties of disks around confirmed members of the Orion OB1 association, 115 belonging to the ~ 10 Myr old 25 Orionis aggregate, and 106 in a region within the ~ 5 Myr old Ori OB1b sub association, near the Orion belt star ϵ Ori. Using optical-2MASS color magnitude diagrams 41 stars were selected as additional photometric candidates of the 25 Orionis aggregate, and 65 as additional photometric candidates of the Ori OB1b field. We use IRAC-MIPS diagrams to detect disk bearing stars, and to classify them as either having no detectable disk emission (class III), as systems with optically-thick disks (class II), or as objects in an intermediate phase between class II and class III systems. These intermediate type objects were further grouped in two categories: “transitional disks candidates”, which have an inner, optically thin disk region combined with an outer, optically thick disk (e.g.; Calvet et al. 2002, 2005b); and “evolved disk objects”, in which there is an overall decrease of emission both the inner and outer regions of the disk (Lada et al. 2006; Hernández et al. 2007). It is not clear if “evolved disks” are a subsequent event after transitional disks phase, or represent an independent evolutionary stage.

We found that the disk frequency in the 25 Orionis aggregate (6 %) and in the Ori OB1b field (13 %) is mass dependent, showing a maximum value for stars with spectral type M0, and suggesting a decrease in the disk frequency toward higher and lower masses. The trend toward higher masses has been observed in several stellar groups (e.g. Hernández et al. 2005; Sicilia-Aguilar et al. 2006; Carpenter et al. 2006). The decrease in disk frequency toward

lower masses is not conclusive, but is consistent with the results for other regions like IC 348 (Lada et al. 2006). We find that objects with evolved disks are more frequent in older stellar groups, while the transitional disk candidates represent a relative small fraction of the disk bearing stars in the various stellar groups, suggesting that the transitional disk phase is relatively fast.

Comparing the disk emission in the IRAC and MIPS bands for Taurus, the σ Orionis cluster, the Ori OB1b field and the 25 Orionis aggregate, we find that disk emission decreases faster in the innermost regions of the disk; comparison with disk models from D’Alessio et al. (2006) support this scenario. Finally, comparing the disk emission in the IRAC spectral range of several stellar groups ranging in age from ~ 1 to ~ 12 Myr, we find that inner disk emission decreases systematically with age, showing a correlation between disk frequencies and inner disk emission. Comparison with models using a typical accretion rate for 1 and 10 Myr suggests that viscous evolution alone is not sufficient to explain the decrease in the inner disk emission, and that large degrees of dust settling ($\epsilon < 0.001$) are necessary to explain the observed SEDs at ages 5 Myr or older.

We thank Massimo Marengo for his advise during the reduction and mosaicking of the IRAC data. This publication makes use of data products from the CIDA Equatorial Variability Survey, obtained with the J. Stock telescope at the Venezuela National Astronomical Observatory, which is operated by CIDA for the Ministerio del Poder Popular para la Ciencia y Tecnología of Venezuela, and from the Two Micron All Sky Survey, which is a joint project of the University of Massachusetts and the Infrared Processing and Analysis Center/California Institute of Technology. This work is based on observations made with the *Spitzer Space Telescope* (GO-1 3437), which is operated by the Jet Propulsion Laboratory, California Institute of Technology under a contract with NASA. Support for this work was provided by NASA grants NAG5-9670 and NAG10545.

REFERENCES

- Alibert, Y., Mordasini, C., & Benz, W. 2004, *A&A*, 417, L25
- Allen, L. E., et al. 2004, *ApJS*, 154, 363
- Baltay, C., et al. 2002, *PASP*, 114, 780
- Baraffe, I., Chabrier, G., Allard, F., & Hauschildt, P. H. 1998, *A&A*, 337, 403

- Briceño, C., Hartmann, L., Stauffer, J., & Martin, E. L. 1998, ASP Conf. Ser. 134: Brown Dwarfs and Extrasolar Planets, 134, 36
- Briceño, C., et al. 2001, *Science*, 291, 93
- Briceño, C., Calvet, N., Hernández, J., Vivas, A. K., Hartmann, L., Downes, J. J., & Berlind, P. 2005, *AJ*, 129, 907.
- Briceño, C., Preibisch, T., Sherry, W. H., Mamajek, E. A., Mathieu, R. D., Walter, F. M., & Zinnecker, H. 2007a, *Protostars and Planets V*, 345
- Briceño, C., Hartmann, L., Hernandez, J., Calvet, N., Katherina Vivas, A., Furesz, G., & Szentgyorgyi, A. 2007a, *ApJ*, 661, 1119.
- Briceño, C., Hartmann, L., Hernandez, J., Calvet, N., Katherina Vivas, A., 2007b, in preparation.
- Brown, A. G. A., Blaauw, A., Hoogerwerf, R., de Bruijne, J. H. J., & de Zeeuw, P. T. 1999, *NATO ASIC Proc. 540: The Origin of Stars and Planetary Systems*, 411
- Calvet, N., D’Alessio, P., Hartmann, L., Wilner, D., Walsh, A., & Sitko, M. 2002, *ApJ*, 568, 1008
- Calvet, N., Briceño, C., Hernández, J., Hoyer, S., Hartmann, L., Sicilia-Aguilar, A., Megeath, S. T., & D’Alessio, P. 2005a, *AJ*, 129, 935
- Calvet, N., et al. 2005b, *ApJ*, 630, L185
- Carpenter, J. M., Mamajek, E. E., Hillenbrand, L. A., & Meyer, M. R. 2006, *ApJ*, 651, 49
- Cutri, R. M., et al. 2003, *VizieR Online Data Catalog*, 2246, 0.
- D’Alessio, P., et al. 2005a, *ApJ*, 621, 461
- D’Alessio, P., Merín, B., Calvet, N., Hartmann, L., & Montesinos, B. 2005b, *Revista Mexicana de Astronomía y Astrofísica*, 41, 61.
- D’Alessio, P., Calvet, N., Hartmann, L., Franco-Hernández, R., & Servín, H. 2006, *ApJ*, 638, 314
- Fabricant, D., Cheimets, P., Caldwell, N., & Geary, J. 1998, *PASP*, 110, 79
- Fabricant, D., et al. 2005, *PASP*, 117, 1411
- Fazio, G. G., et al. 2004, *ApJS*, 154, 39

- Furlan, E., et al. 2006, *ApJS*, 165, 568
- Gordon, K. D., et al. 2005, *PASP*, 117, 503
- Gorlova, N., Rieke, G. H., Muzerolle, J., Stauffer, J. R., Siegler, N., Young, E. T., & Stansberry, J. H. 2006, *ApJ*, 649, 1028
- Gutermuth, R. A., Megeath, S. T., Muzerolle, J., Allen, L. E., Pipher, J. L., Myers, P. C., & Fazio, G. G. 2004, *ApJS*, 154, 374
- Haisch, K. E., Lada, E. A., & Lada, C. J. 2001, *ApJ*, 553, L153
- Hartmann, L., Calvet, N., Gullbring, E., & D'Alessio, P. 1998, *ApJ*, 495, 385
- Hartmann, L. 2003, *ApJ*, 585, 398
- Hartmann, L. 2005, *ASP Conf. Ser.* 341: Chondrites and the Protoplanetary Disk, 341, 131
- Hartmann, L., Megeath, S. T., Allen, L., Luhman, K., Calvet, N., D'Alessio, P., Franco-Hernandez, R., & Fazio, G. 2005, *ApJ*, 629, 881
- Hernández, J., Calvet, N., Hartmann, L., Briceño, C., Sicilia-Aguilar, A., & Berlind, P. 2005, *AJ*, 129, 856.
- Hernández, J., Briceño, C., Calvet, N., Hartmann, L., Muzerolle, J., & Quintero, A. 2006, *ApJ*, 652, 472
- Hernandez, J., et al. 2007, *ApJ*, 662, 1067.
- Kenyon, M. J., Jeffries, R. D., Naylor, T., Oliveira, J. M., & Maxted, P. F. L. 2005, *MNRAS*, 356, 89
- Kenyon, S. J. & Hartmann, L. 1995, *ApJS*, 101, 117
- Lada, E. A., & Lada, C. J. 1995, *AJ*, 109, 1682
- Lada, C. J., et al. 2006, *AJ*, 131, 1574
- Lee, H.-T., & Chen, W. P. 2007, *ApJ*, 657, 884
- Lyra, W., Moitinho, A., van der Blik, N. S., & Alves, J. 2006, *A&A*, 453, 101
- Megeath, S. T., et al. 2004, *ApJS*, 154, 367
- Megeath, S. T., Allen, L. E., Allgaier, E., Muzerolle, J., Peterson, D. E., Siegler, N., Wilson, T. L., & Young, E. C. 2006, *IAU Symposium*, 237

- Muzerolle, J., Calvet, N., Briceño, C., Hartmann, L., & Hillenbrand, L. 2000, *ApJ*, 535, L47
- Muzerolle, J., et al. 2004, *ApJS*, 154, 379.
- Pollack, J. B., Hubickyj, O., Bodenheimer, P., Lissauer, J. J., Podolak, M., & Greenzweig, Y. 1996, *Icarus*, 124, 62
- Preibisch, T., & Zinnecker, H. 2006, *ArXiv Astrophysics e-prints*, arXiv:astro-ph/0610826
- Reach, W. et al. 2006, *Infrared Array Camera Data Handbook*, version 3.0, *Spitzer Science Center*, California Institute of Technology, Pasadena, California 91125 USA.
- Rieke, G. H., et al, 2004, *ApJS*, 154, 25
- Schlegel, D. J., Finkbeiner, D. P., & Davis, M. 1998, *ApJ*, 500, 525
- Schuster, M. T., Marengo, M., & Patten, B. M. 2006, *Proc. SPIE*, 6270, 65.
- Sicilia-Aguilar, A., Hartmann, L. W., Hernández, J., Briceño, C., & Calvet, N. 2005, *AJ*, 130, 188
- Sicilia-Aguilar, A., et al. 2006, *ApJ*, 638, 897
- Siess, L., Dufour, E., & Forestini, M. 2000, *A&A*, 358, 593
- Uchida, K. I., et al. 2004, *ApJS*, 154, 439
- Vivas, A. K., et al. 2004, *AJ*, 127, 1158
- White, R. J., & Basri, G. 2003, *ApJ*, 582, 1109
- Young, E. T., et al. 2006, *ApJ*, 642, 972

Table 1. Members of the 25 Orionis aggregate

OB1a ID	2MASS ID	RA(2000) deg	DEC(2000) deg	[3.6] mag	[4.5] mag	[5.8] mag	[8.0] mag	[24.0] mag	Ref opt	Disk types
9	05224654+0134010	80.69393	1.56697	12.419 ± 0.030	12.629 ± 0.131	12.275 ± 0.036	12.458 ± 0.042	... ± ...	3	CIII
25	05224842+0140438	80.70176	1.67885	12.817 ± 0.030	12.777 ± 0.031	12.753 ± 0.041	12.824 ± 0.057	... ± ...	3	CIII
47	05225186+0145132	80.71609	1.75367	13.269 ± 0.031	13.262 ± 0.032	13.139 ± 0.050	13.450 ± 0.112	... ± ...	3	CIII
53	05225304+0152151	80.72102	1.87088	12.416 ± 0.030	12.348 ± 0.031	12.240 ± 0.036	12.258 ± 0.043	... ± ...	3	CIII
905	05245885+0125183	81.24523	1.42177	12.904 ± 0.031	12.724 ± 0.031	12.456 ± 0.037	11.889 ± 0.040	9.20 ± 0.04	3	EV
930	05250192+0134563	81.25801	1.58232	11.720 ± 0.030	11.865 ± 0.030	11.562 ± 0.032	11.825 ± 0.036	... ± ...	2	CIII
931	05250205+0137210	81.25855	1.62252	11.435 ± 0.030	11.228 ± 0.030	11.326 ± 0.032	11.137 ± 0.033	... ± ...	1	disk[8]?
948	05250362+0144121	81.26511	1.73670	11.949 ± 0.030	12.061 ± 0.030	11.831 ± 0.034	11.876 ± 0.036	... ± ...	2	CIII

Note. — Table 1 is published in its entirety in the electronic edition of the *Astrophysical Journal*. A portion is shown here for guidance regarding its form and content.

References in column 10: 1 Briceño et al. (2005); 2 Briceño et al. (2007b); 3 Briceño et al. (2007c)

Disk types: CIII:disk less stars; CII:optically thick disks; EV:evolved disks; TD: transitional disk candidates; disk[8]?:excess at 8 μ m but no MIPS detections.

Table 2. Members of the OB1b field

OB1b ID	2MASS ID	RA(2000) deg	DEC(2000) deg	[3.6] mag	[4.5] mag	[5.8] mag	[8.0] mag	[24.0] mag	Ref opt	Disk type
21	05290540-0127500	82.27250	-1.46390	11.830 ± 0.030	11.865 ± 0.030	11.787 ± 0.034	11.846 ± 0.038	... ± ...	3	CIII
31	05290635-0152122	82.27648	-1.87008	12.751 ± 0.030	12.707 ± 0.031	12.632 ± 0.040	12.595 ± 0.057	... ± ...	3	CIII
63	05290882-0125393	82.28679	-1.42760	11.268 ± 0.030	11.291 ± 0.030	11.221 ± 0.032	11.076 ± 0.033	... ± ...	1	CIII
70	05290925-0121227	82.28856	-1.35633	12.383 ± 0.030	12.291 ± 0.031	12.122 ± 0.035	11.813 ± 0.038	... ± ...	3	CIII
78	05291078-0117281	82.29495	-1.29115	12.004 ± 0.030	11.989 ± 0.030	11.906 ± 0.034	11.974 ± 0.040	... ± ...	3	CIII
89	05291202-0112236	82.30010	-1.20657	13.138 ± 0.031	13.085 ± 0.031	13.120 ± 0.052	13.067 ± 0.089	... ± ...	3	CIII
148	05291821-0204066	82.32590	-2.06852	11.267 ± 0.030	11.152 ± 0.030	11.058 ± 0.032	10.917 ± 0.034	... ± ...	3	CIII
209	05292326-0125153	82.34693	-1.42092	9.457 ± 0.030	9.238 ± 0.030	8.809 ± 0.030	8.392 ± 0.030	5.23 ± 0.03	1	CII

Note. — Table 2 is published in its entirety in the electronic edition of the *Astrophysical Journal*. A portion is shown here for guidance regarding its form and content.

References in column 10: 1 Briceño et al. (2005); 2 Briceño et al. (2007b); 3 Briceño et al. (2007c)

Disk types: CIII:disk less stars; CII:optically thick disks; EV:evolved disks; TD: transitional disk candidates; disk[8]?:excess at 8 μ m but no MIPS detections.

Table 3. Photometric candidates of the 25 Orionis aggregate

OB1a ID	2MASS ID	RA(2000) deg	DEC(2000) deg	[3.6] mag	[4.5] mag	[5.8] mag	[8.0] mag	[24.0] mag	V mag	VI mag	Disk type
146	05230905+0125355	80.78774	1.42654	11.383 ± 0.030	11.355 ± 0.030	11.278 ± 0.032	11.284 ± 0.034	... ± ...	15.75 ± 0.04	2.43 ± 0.05	CIII
297	05233109+0144079	80.87958	1.73555	11.005 ± 0.030	11.079 ± 0.030	11.028 ± 0.031	10.967 ± 0.032	... ± ...	13.91 ± 0.03	1.06 ± 0.05	CIII
359	05234182+0152261	80.92428	1.87394	13.144 ± 0.031	13.088 ± 0.031	12.986 ± 0.041	13.039 ± 0.055	... ± ...	19.11 ± 0.05	3.09 ± 0.09	CIII
427	05235215+0136314	80.96732	1.60873	11.103 ± 0.030	11.191 ± 0.030	11.155 ± 0.032	11.074 ± 0.032	... ± ...	13.84 ± 0.03	0.98 ± 0.05	CIII
458	05235854+0151255	80.99394	1.85709	12.114 ± 0.030	12.047 ± 0.030	12.003 ± 0.034	12.043 ± 0.040	... ± ...	17.29 ± 0.04	2.58 ± 0.07	CIII
477	05240118+0128236	81.00493	1.47324	12.316 ± 0.030	12.289 ± 0.031	12.123 ± 0.035	12.165 ± 0.041	... ± ...	16.87 ± 0.04	2.49 ± 0.06	CIII
543	05241034+0155024	81.04312	1.91735	10.322 ± 0.030	10.428 ± 0.030	10.365 ± 0.031	10.309 ± 0.031	... ± ...	13.16 ± 0.03	0.80 ± 0.05	CIII
1626	05265473+0144337	81.72806	1.74271	10.168 ± 0.030	10.273 ± 0.030	10.061 ± 0.031	10.069 ± 0.031	9.83 ± 0.06	13.43 ± 0.03	0.86 ± 0.05	EV

Note. — Table 3 is published in its entirety in the electronic edition of the *Astrophysical Journal*. A portion is shown here for guidance regarding its form and content.

Disk types: CIII:disk less stars; CII:optically thick disks; EV:evolved disks; TD: transitional disk candidates; disk[8]?:excess at 8 μ m but no MIPS detections.

Table 4. Photometric candidates of the OB1b field

OB1b ID	2MASS ID	RA(2000) deg	DEC(2000) deg	[3.6] mag	[4.5] mag	[5.8] mag	[8.0] mag	[24.0] mag	V mag	VI mag	Disk type
74	05290984-0208250	82.29101	-2.14030	12.269 ± 0.030	12.217 ± 0.031	12.141 ± 0.036	12.113 ± 0.042	... ± ...	18.26 ± 0.05	2.89 ± 0.09	CIII
187	05292160-0201546	82.34002	-2.03184	11.142 ± 0.030	11.121 ± 0.030	11.073 ± 0.031	11.025 ± 0.034	... ± ...	15.91 ± 0.06	2.04 ± 0.09	CIII
203	05292300-0126559	82.34584	-1.44888	13.500 ± 0.131	13.262 ± 0.032	13.186 ± 0.042	13.184 ± 0.085	... ± ...	18.89 ± 0.05	2.83 ± 0.08	CIII
207	05292313-0149203	82.34638	-1.82231	13.109 ± 0.031	13.105 ± 0.031	13.059 ± 0.051	13.451 ± 0.153	... ± ...	18.83 ± 0.05	2.63 ± 0.08	CIII
222	05292426-0207354	82.35112	-2.12651	12.953 ± 0.031	13.055 ± 0.031	12.730 ± 0.042	12.825 ± 0.063	... ± ...	17.78 ± 0.05	2.27 ± 0.08	CIII
236	05292591-0144580	82.35797	-1.74945	10.810 ± 0.030	10.832 ± 0.030	10.757 ± 0.031	10.707 ± 0.032	... ± ...	14.64 ± 0.04	1.41 ± 0.06	CIII
276	05293010-0114446	82.37544	-1.24573	11.116 ± 0.030	11.217 ± 0.030	11.175 ± 0.032	11.107 ± 0.034	... ± ...	14.37 ± 0.00	1.25 ± 0.00	CIII
283	05293049-0121500	82.37707	-1.36389	11.303 ± 0.030	11.376 ± 0.030	11.314 ± 0.032	11.309 ± 0.036	... ± ...	14.56 ± 0.04	1.30 ± 0.06	CIII
342	05293578-0148046	82.39909	-1.80129	11.138 ± 0.030	11.185 ± 0.030	11.129 ± 0.031	11.144 ± 0.034	...			

Note. — Table 4 is published in its entirety in the electronic edition of the *Astrophysical Journal*. A portion is shown here for guidance regarding its form and content.

Disk types: CIII:disk less stars; CII:optically thick disks; EV:evolved disks; TD: transitional disk candidates; disk[8]?:excess at 8 μ m but no MIPS detections.

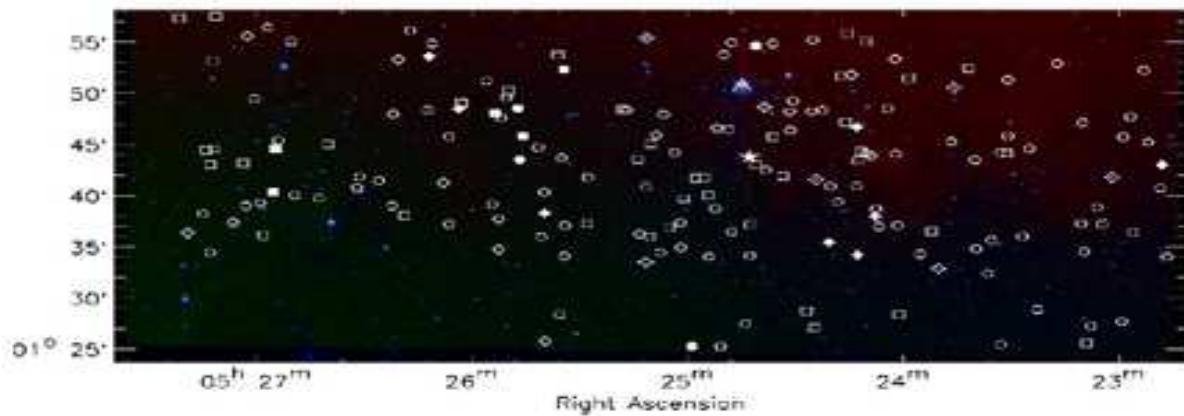


Fig. 1.— IRAC image of the 25 Orionis aggregate. This is a 3-color composite of IRAC images (3.6 (blue), 4.5 (green), and 8.0 (red) μm) illustrating the space distribution of members in this aggregate. Circles represent stars confirmed as low mass members using spectroscopic data (Briceño et al. 2005, 2007b,c), squares represent photometric low mass candidates of 25 Orionis. Solid symbols indicate stars bearing disks (see §3.1). Intermediate mass members selected in Hernández et al. (2006) are represented as diamonds, open symbols represent stars without disks and solid symbols represent debris disk candidates. The star indicates the Herbig Ae star V346 Ori (Hernández et al. 2006) and the triangle indicates the Be star 25 Ori.[See electronic edition of ApJ for a color version of this figure.]

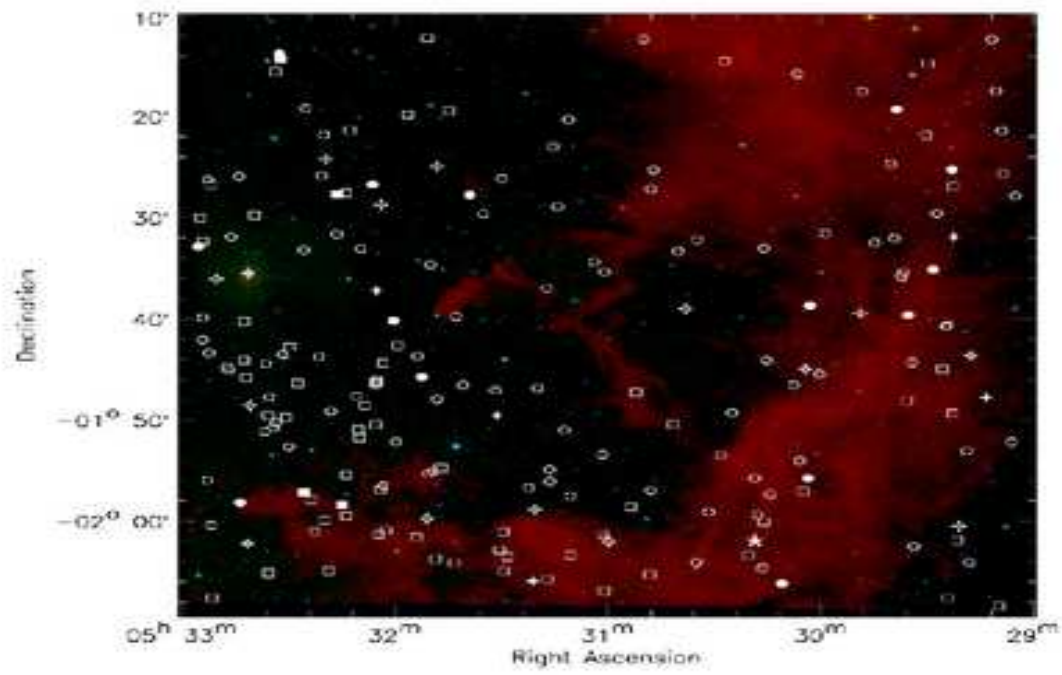


Fig. 2.— IRAC image of the OB1b region. This is a 3-color composite of IRAC images, 3.6 (blue), 4.5 (green), and 8.0 (red) μm . Symbols are as in Figure 1. The star indicates the Herbig Ae star HD290543 (Hernández et al. 2006)[See electronic edition of ApJ for a color version of this figure.]

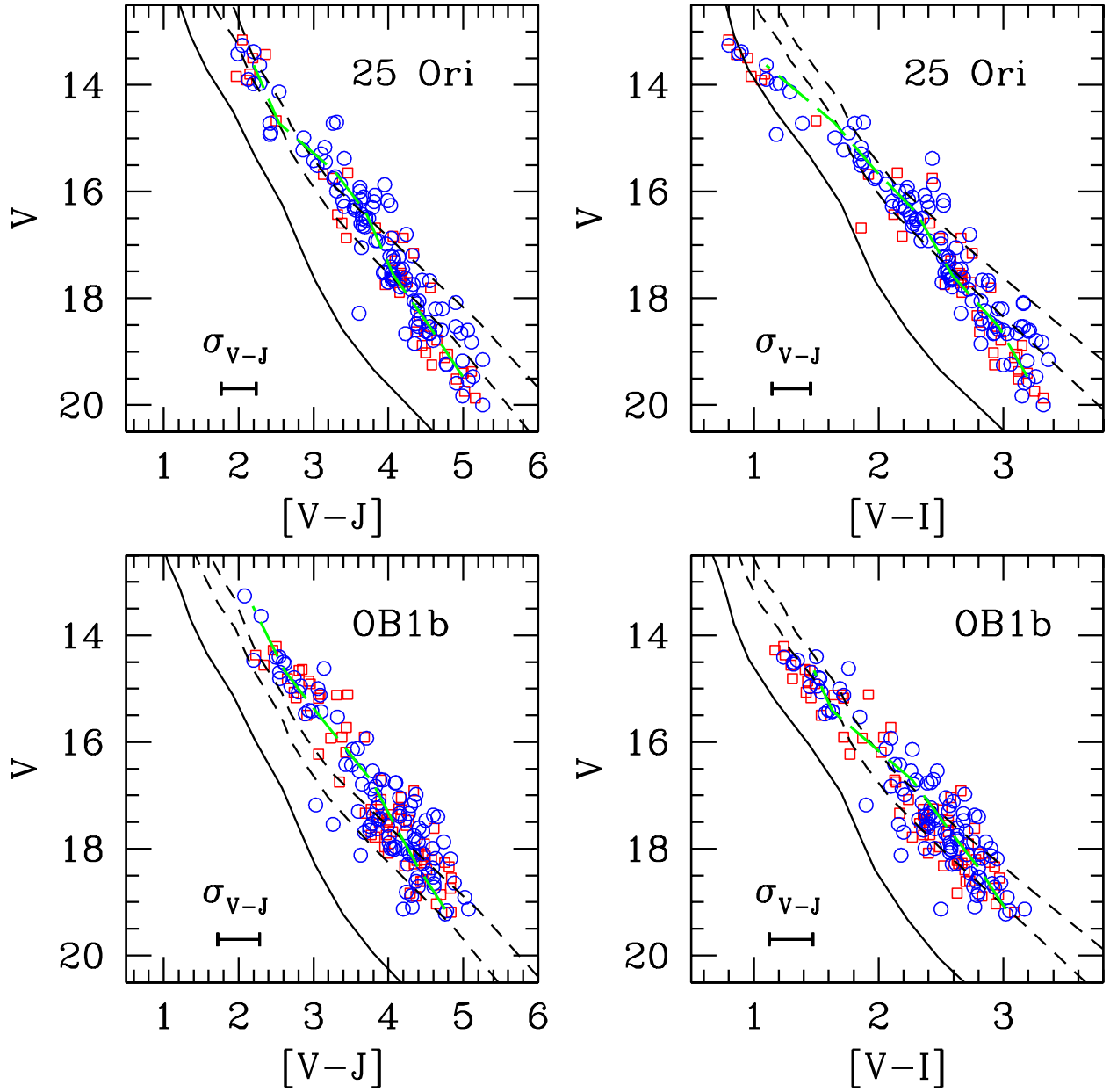


Fig. 3.— Color magnitude diagrams illustrating the selection of low mass photometric candidates in 25 Orionis (upper panels) and in OB1b (lower panels). Photometric candidates (open squares) have similar distribution than members (open circles) confirmed using spectroscopic methods (Briceño et al. 2005, 2007b,c). By comparison, the ZAMS (solid lines) and the isochrones at 10 Myr and 5 Myr (dashed lines; Siess et al. 2000) are displayed at the distance of each stellar group; 330 pc for 25 Orionis and 440 pc for OB1b (Briceño et al. 2005, 2007b; Hernández et al. 2005). Long dashed lines represent the median colors for the spectroscopic members.[See electronic edition of ApJ for a color version of this figure.]

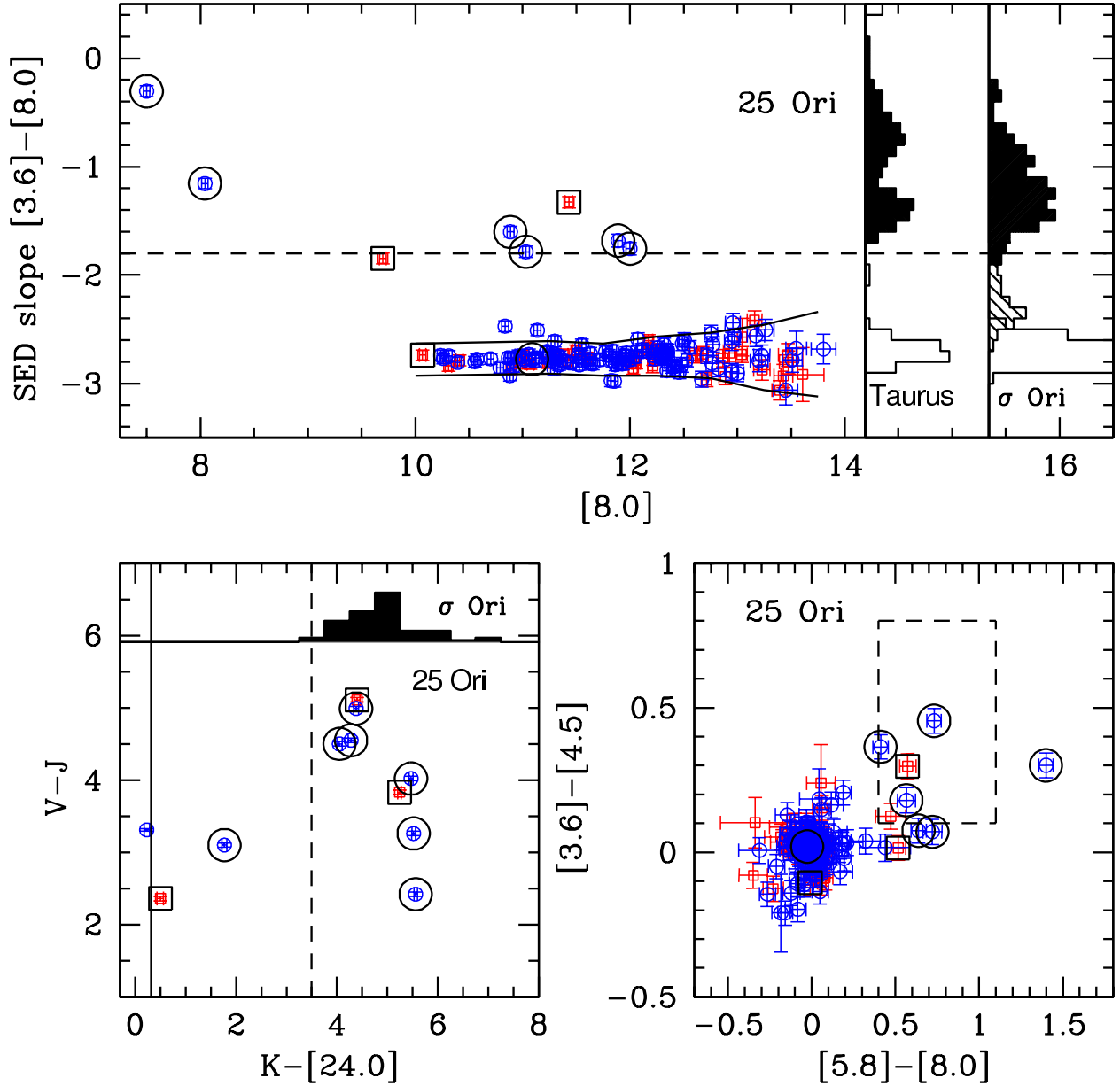


Fig. 4.— Diagrams illustrating the detection of sources with infrared excess above the photospheric levels (solid lines) in 25 Orionis. The top panel shows the IRAC SED slope diagram indicating stars with excess at $8 \mu\text{m}$. The bottom-left panel shows a 2MASS-MIPS color-color diagram indicating stars with excess emission at the MIPS $24 \mu\text{m}$ band. The bottom-right panel shows an IRAC color-color diagram indicating objects with infrared excess at $[4.5]$ and $[8.0]$. Members and photometric candidates are displayed as circles and squares, respectively. Large circles and large squares represent stars with infrared excess at $24 \mu\text{m}$. The solid histograms represent the distribution of IRAC SED slopes for stars with optically thick disks in Taurus (Hartmann et al. 2005) and in the σ Orionis cluster (Hernández et al. 2007); dashed lines represent the class II region limit based on these histograms. The open histograms represent the distribution of stars with no IRAC excesses. The dashed histogram is the distribution of stars with evolved disks in the σ Orionis cluster (Hernández et al. 2007)[See electronic edition of ApJ for a color version of this figure.]

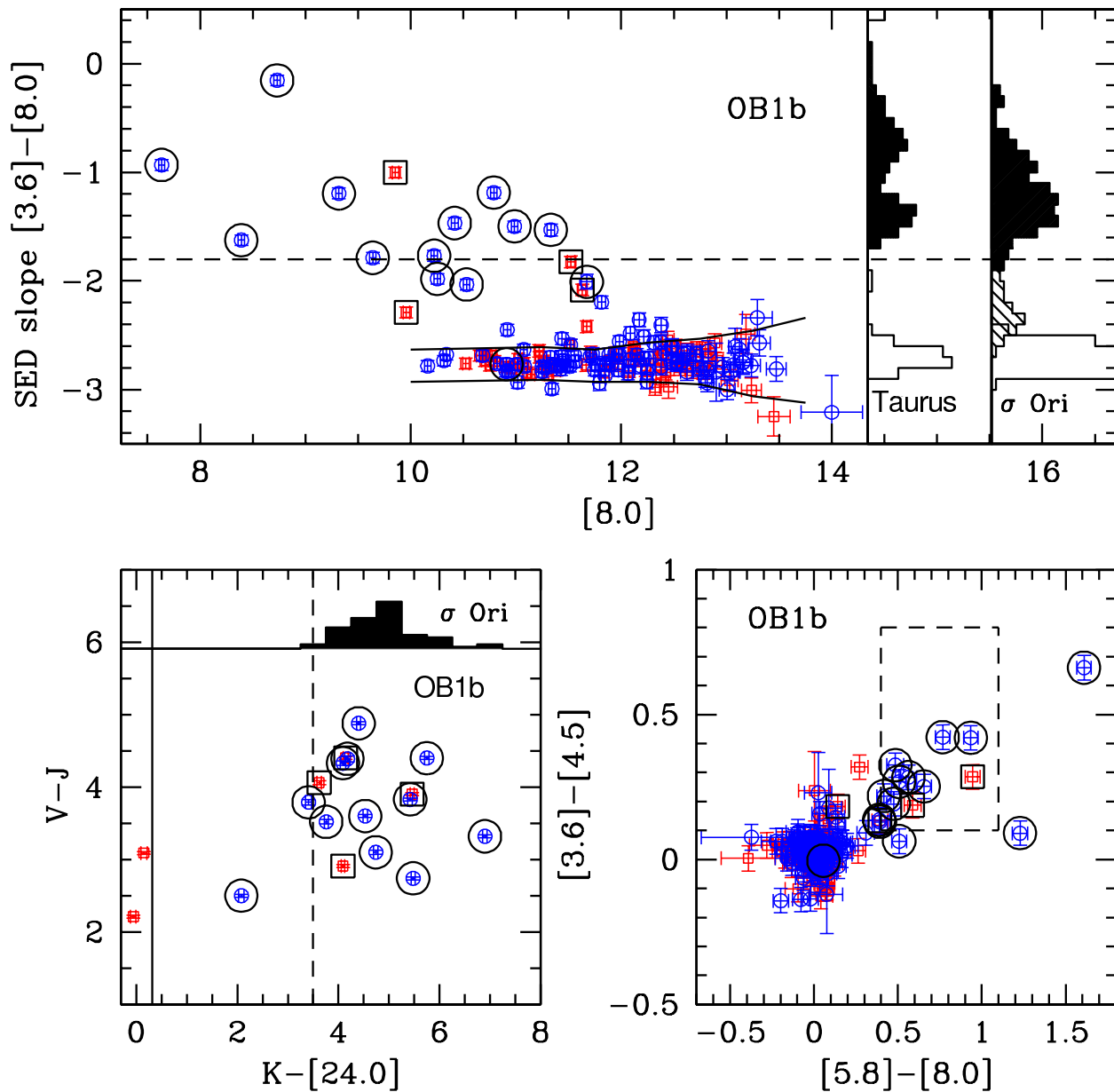


Fig. 5.— Diagrams illustrating the detection of sources with infrared excess above the photospheric levels (solid lines) in the OB1b field. Symbols are similar to Figure 4.[See electronic edition of ApJ for a color version of this figure.]

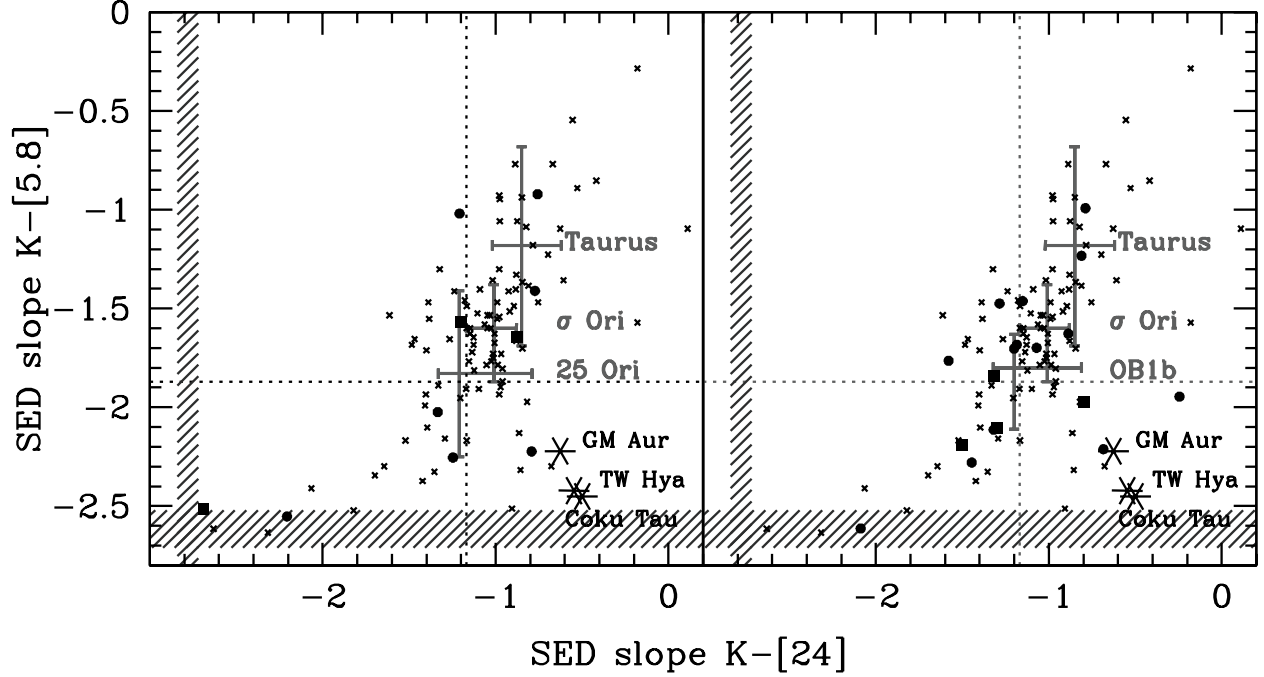


Fig. 6.— SED slope K-[5.8] versus SED slope K-[24] for members (circles) and photometric candidates (squares) bearing disks in 25 Orionis (left panel) and in OB1b (right panel). Error bars represent the quartiles of the stellar groups, Taurus (1 Myr), the σ Orionis cluster (3 Myr), OB1b (5 Myr), and 25 Orionis (10 Myr). Stars represent the transitional disk objects, Coku Tau4, TW Hya, and GM Aur (D’Alessio et al. 2005a; Uchida et al. 2004; Calvet et al. 2002, 2005b). Photospheric regions derived for K5-M5 stars using STAR-PET *Spitzer* tool are represented as dashed areas. Disk bearing stars in the σ Orionis cluster (Hernández et al. 2007) are represented with the symbol X. The horizontal dotted line represents the lower quartile of the stars bearing disks in the σ Orionis cluster, $\sim 96\%$ of stars with disks in Taurus are located above this line; we define the area above this line as the class II region (CII in Table 1-4). The vertical dotted line represents the lower quartile of the stars bearing disks in the σ Orionis cluster. We use this limit to separate transitional disk candidate (TD in Table 1-4) from stars with evolved disks (EV in Table 1-4).

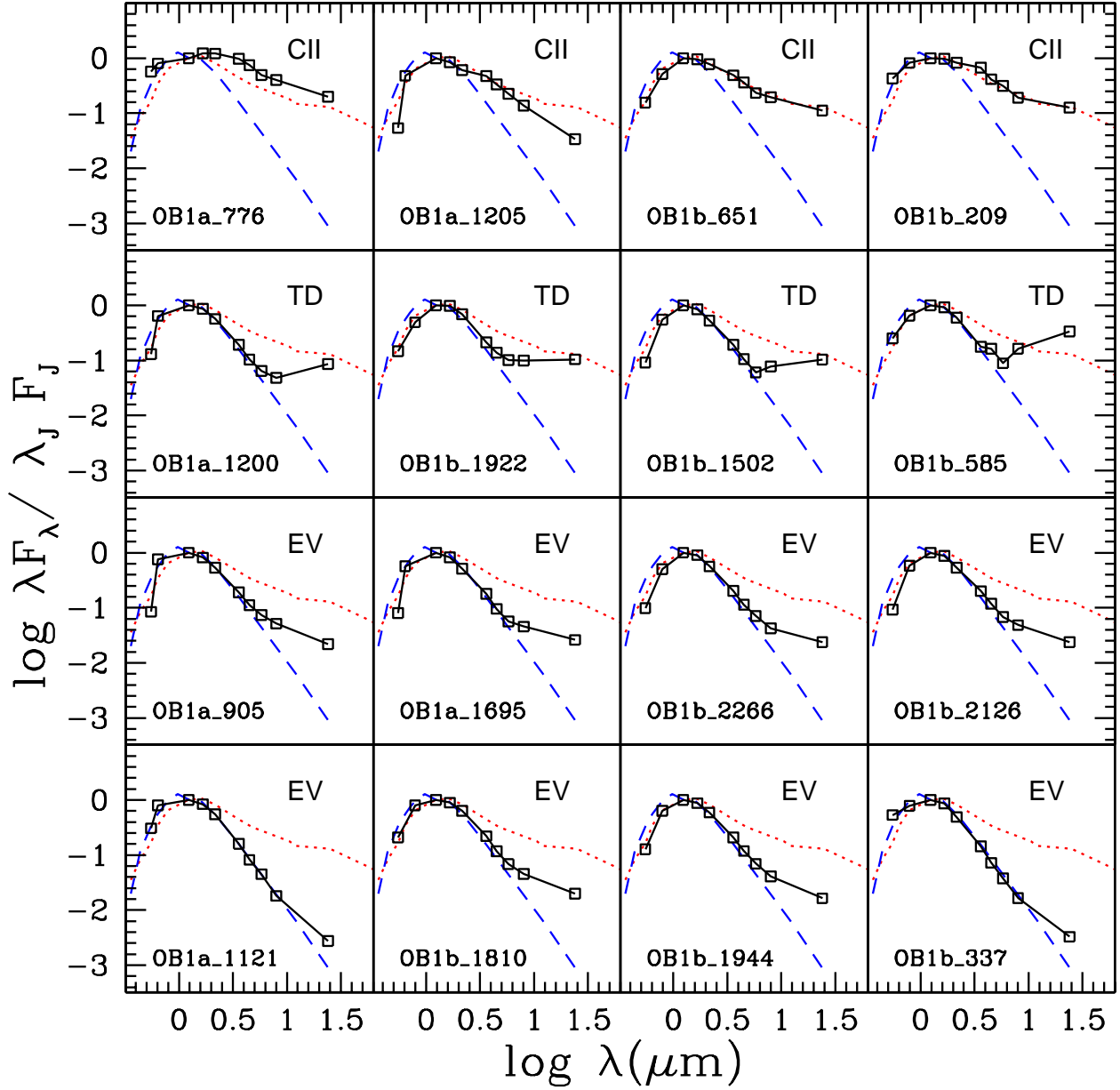


Fig. 7.— Spectral energy distributions for selected disk bearing stars, illustrating the diversity of disks found at 5 and 10 Myr. Dotted line represents the median SEDs of disk bearing stars in Taurus (Hartmann et al. 2005). Dashed line represents the median photosphere of stars in the spectral type range K5-M5 (Kenyon & Hartmann 1995). We display examples of the disk types found in Figure 6: stars with optically thick disks (CII), transitional disk candidates (TD) and evolved disks objects (EV).[See electronic edition of ApJ for a color version of this figure.]

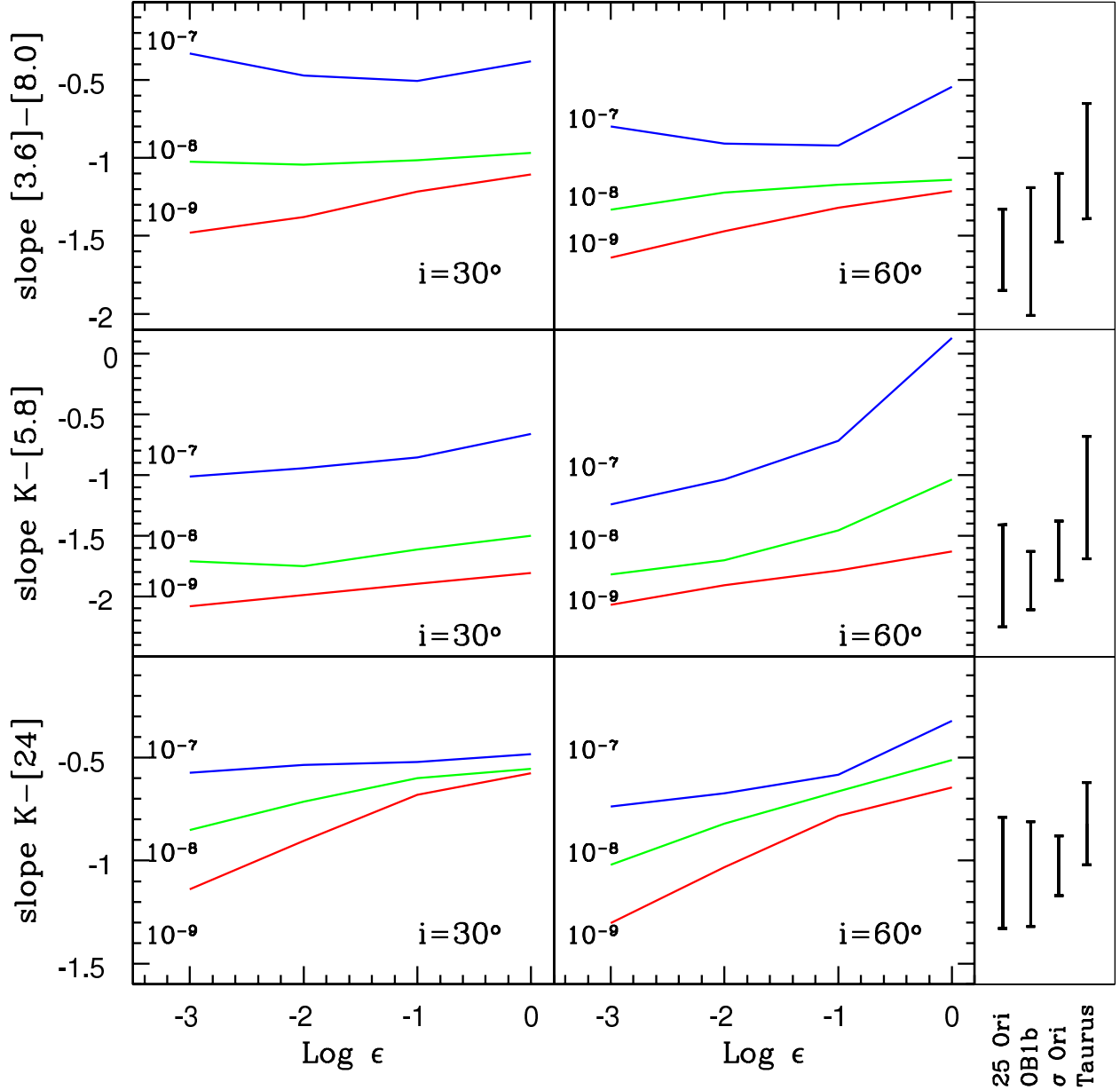


Fig. 8.— Theoretical SED slopes as function of the degree of settling. Each panel shows three curves corresponding to different accretion rates ($\dot{M}=10^{-7}$, $\dot{M}=10^{-8}$ and $\dot{M}=10^{-9}$). The parameter ϵ represents the degree of settling in each model. The central object is a typical T Tauri star with $M=0.6M_{\odot}$, Age=1 Myr, corresponding to a spectral type K7 (Siess et al. 2000). Left and middle panels represent disks oriented with an angle of 30deg and 60 deg, respectively. In the right panels, we display the quartiles of the disk population in Taurus (1-2 Myr; Hartmann et al. 2005; Furlan et al. 2006), the σ Orionis cluster (~ 3 Myr Hernández et al. 2007), and the stellar groups studied in this contribution, OB1b (~ 5 Myr) and 25 Orionis (~ 10 Myr). [See electronic edition of ApJ for a color version of this figure.]

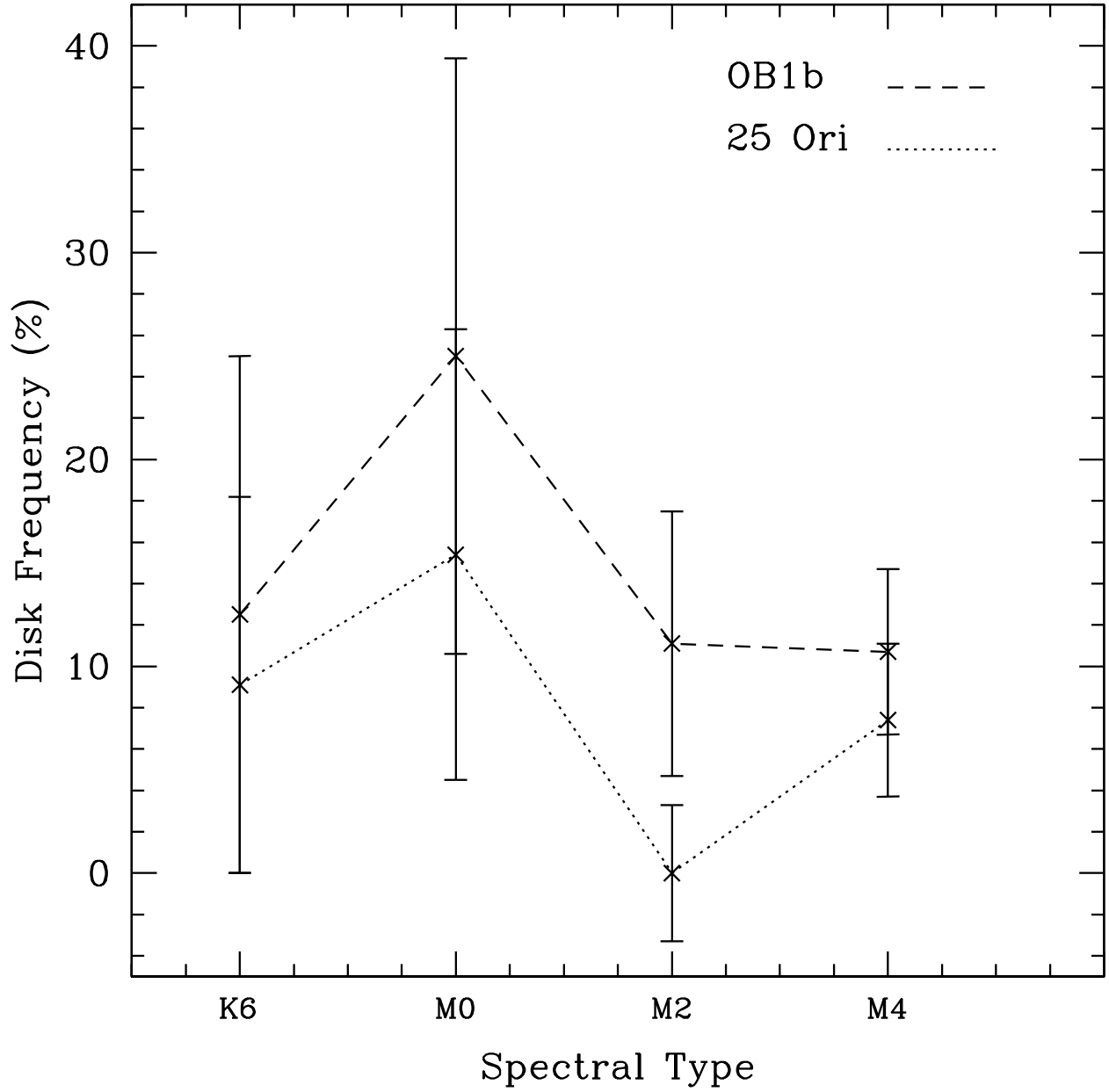


Fig. 9.— Disk frequency as function of spectral type for the 25 Orionis aggregate (dotted line) and the OB1b field (dashed line). The error bars represent the Poissonian statistical uncertainties

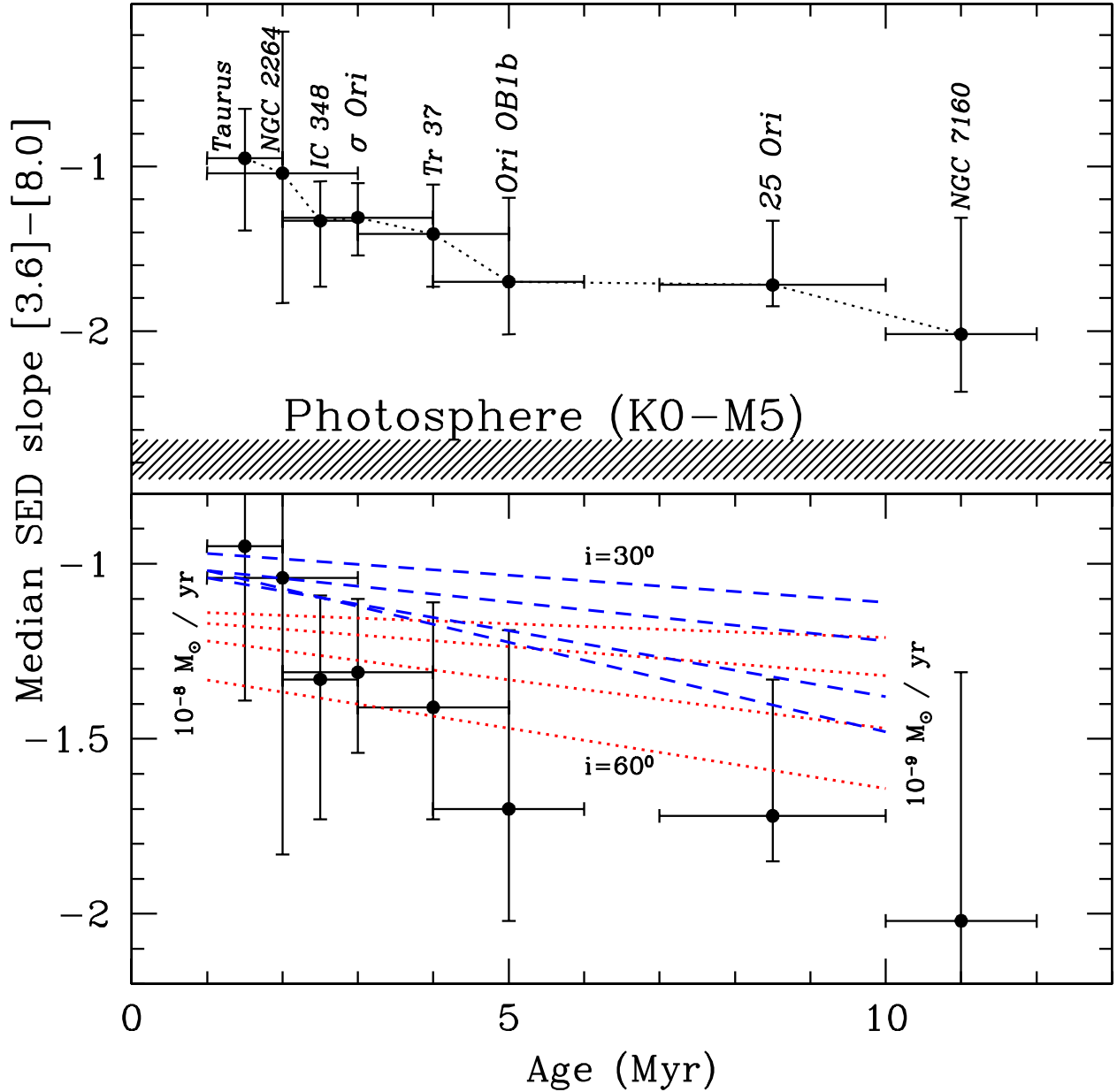


Fig. 10.— Median SED slope in the IRAC spectral range versus stellar ages of different stellar groups: Taurus (Hartmann et al. 2005), NGC 2264 (Young et al. 2004), IC 348 (Lada et al. 2006), σ Orionis (Hernández et al. 2007), Tr37 and NGC 7160 (Sicilia-Aguilar et al. 2006), and 25 Orionis and OB1b (Briceño et al. 2007b, and this work). The dashed region indicates the photospheric levels estimated using STAR-PET *Spitzer* tool. It is apparent that the infrared disk emission decreases with the age of the stellar groups. The lower panel shows a comparison with theoretical values described in §3.2. Two set of models are displayed showing different orientation of the disks, 30 deg (dashed lines) and 60 deg (dotted lines). We assume canonical values for accretion rate at 1 Myr and 10 Myr (see text). Different lines describe different degree of settling ($\epsilon=1,0.1,0.01$ and 0.001) showing flatter slopes for models with less degree of settling.[See electronic edition of ApJ for a color version of this figure.]

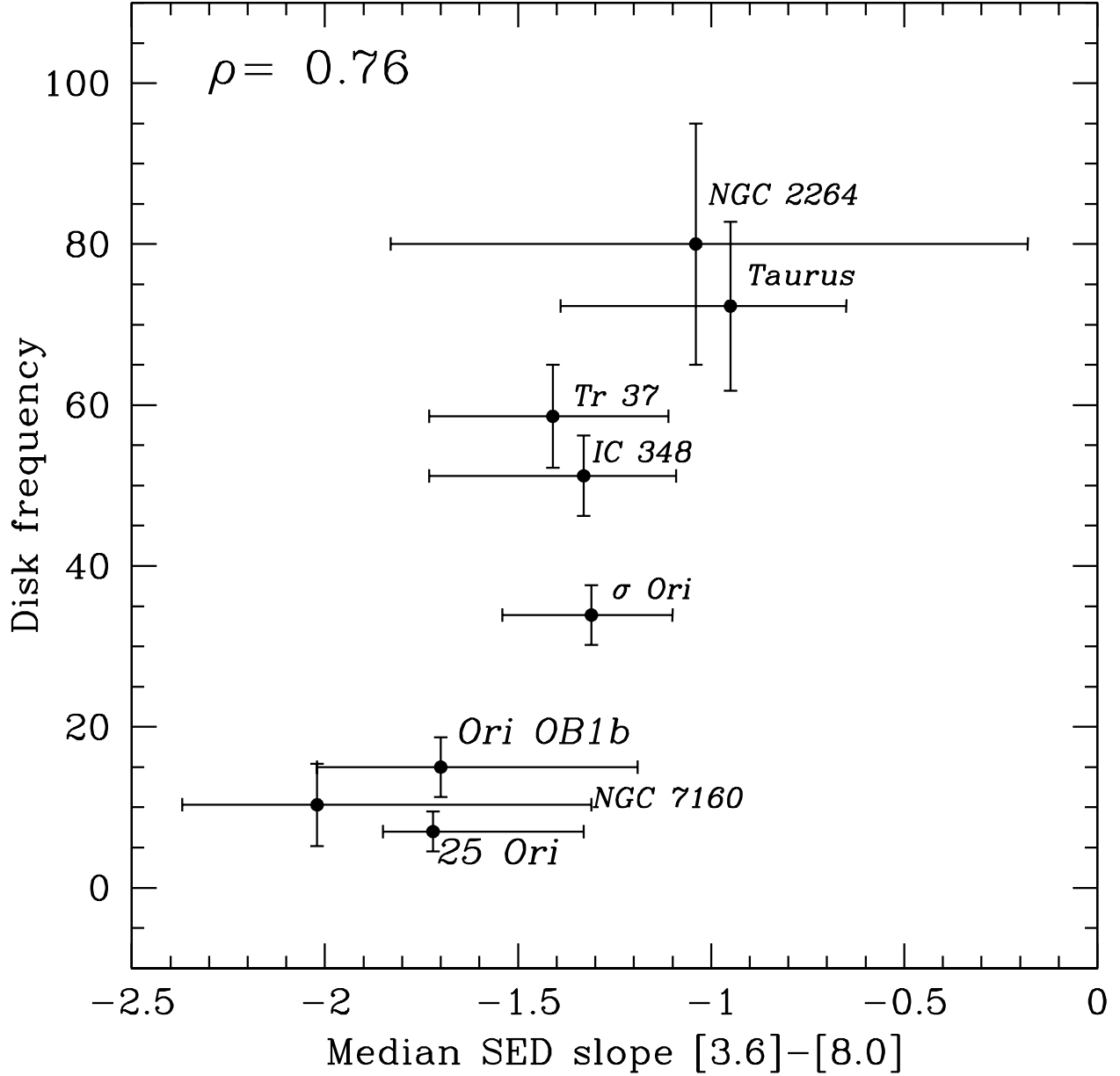


Fig. 11.— IRAC disk Frequency versus the median SED slope [3.6]–[8.0] for different stellar groups (see Figure 10). These measurements are correlated (correlation coefficient $\rho=0.76$) indicating more flaring disks in stellar groups with higher disk frequency.